Thermolytic Transformation of Tris(alkoxy)siloxychromium(IV) Single-Source Molecular Precursors to Catalytic Chromia−Silica Materials

Kyle L. Fujdala and T. Don Tilley*

Department of Chemistry, University of California, Berkeley, Berkeley, California 94720-1460, and the Chemical Sciences Division, Lawrence Berkeley Laboratory, 1 Cyclotron Road, Berkeley, California 94720

Received January 9, 2001. Revised Manuscript Received March 8, 2001

Reactions of 1 and 2 equiv of $HOSi(O^tBu)_3$ with $Cr(O^tBu)_4$ afforded the first Cr(IV) alkoxysiloxy complexes $(^tBuO)_3CrOSi(O^tBu)_3$ (**1**) and $(^tBuO)_2Cr[OSi(O^tBu)_3]_2$ (**2**), respectively. Both **1** and **2** contain pseudotetrahedral d^2 chromium centers and crystallize in the monoclinic space group $P2_1/n$ with four molecules in the unit cell. The high-yielding, convenient synthesis of **1** makes this complex a useful single-source molecular precursor, via the *thermolytic molecular precursor* method, to Cr/Si/O materials. The thermal transformations of **1** and **2** to chromia−silica materials occurred at low temperatures (≤180 °C), to give isobutene as the major carbon-containing product. The material generated from the solid-state conversion of **1** ($\mathbf{CrOSi_{ss}}$) contained both micro- and mesoporosity with an unexpectedly high surface area of 315 m^2/g that was slightly reduced to 275 m^2/g after calcination at 500 °C in O_2. The xerogel obtained by the thermolysis of an *n*-octane solution of **1** ($\mathbf{CrOSi_{xg}}$) had a surface area of 315 m^2/g that was reduced to 205 m^2/g upon calcination at 500 °C. The nitrogen adsorption−desorption isotherm for the xerogel had characteristics indicating both microporosity and textural mesoporosity. Powder X-ray diffraction (PXRD) analysis was used to demonstrate that Cr_2O_3 was the only species that crystallized in $\mathbf{CrOSi_{ss}}$ and $\mathbf{CrOSi_{xg}}$ after calcination at temperatures up to 1200 °C in O_2. Elemental analyses of these materials revealed that the Cr:Si ratio was very close to 1:1, indicating that the original stoichiometry of the precursor is retained upon thermal conversion to Cr/Si/O materials. Both materials contained very low amounts of carbon after calcination in O_2 at 500 °C. In the oxidative dehydrogenation of propane, $\mathbf{CrOSi_{xg}}$ (calcined at 500 °C) displayed intrinsic activities for propene formation that were up to 3 times higher than those for $\mathbf{CrOSi_{ss}}$ (calcined at 500 °C). In addition, the selectivity for propene formation was higher for the more active $\mathbf{CrOSi_{xg}}$ catalyst.

Introduction

The development of synthetic methods that allow fine control over solid-state structures at the atomic level is a fundamental goal in materials science.[1] In this context, there has been significant interest in low-temperature routes to metastable structures. A widely used low-temperature method for the preparation of oxide materials is the sol−gel process, which involves the hydrolysis and condensation of metal alkoxide precursors, typically in polar media (such as ROH or H_2O).[2] However, use of the sol−gel process to synthesize homogeneous mixed-metal oxides is plagued by differences in the hydrolysis rates of the metal alkoxide precursors, which can lead to heterogeneous mixtures.[2,3] An alternative approach for the preparation of oxide materials involves the use of single-source molecular precursors that possess a defined ratio of elements.[4] Advantages of the single-source molecular precursor route include the efficient incorporation of fundamental building blocks, well-defined stoichiometries, and low-temperature, kinetically controlled routes to metastable structures.

---

(1) (a) *Ultrastructure Processing of Advanced Materials*; Uhlmann, D. R., Ulrich, D. R., Eds.; Wiley-Interscience: New York, 1992. (b) *Better Ceramics Through Chemistry VI*; Cheetham, A. K., Brinker, C. J., Mecartney, M. L., Sanchez, C., Eds.; Materials Research Society Symposium Proceedings Vol. 360; Materials Research Society: Pittsburgh, 1994, and previous volumes. (c) *Inorganic Materials*; Bruce, D. W., O'Hare, D., Eds; Wiley: New York, 1992. (d) Bowes, C. L.; Ozin, G. A. *Adv. Mater.* **1996**, *8*, 13. (e) Stein, A.; Keller, S. W.; Mallouk, T. E. *Science* **1993**, *259*, 1558. (f) Mehrotra, R. C. *J. Non-Cryst. Solids* **1988**, *100*, 1. (g) Amabilino, D. B.; Stoddart, J. F. *Chem. Rev.* **1995**, *95*, 2725.

(2) (a) Brinker, C. J.; Scherer, G. W. *Sol−Gel Science*; Academic Press: Boston, 1990. (b) *Sol−Gel Technology for Thin Films, Fibers, Preforms, Electronics, and Specialty Shapes*; Klein, L. C., Ed.; Noyes: Park Ridge, NJ, 1988. (c) Brinker, C. J. *J. Non-Cryst. Solids* **1988**, *100*, 31. (d) Corriu, R. J. P.; Leclercq, D. *Angew. Chem., Int. Ed. Engl.* **1996**, *35*, 1421. (e) Schmidt, H. *J. Non-Cryst. Solids* **1988**, *100*, 51.

(3) (a) Schubert, U. *J. Chem. Soc., Dalton Trans.* **1996**, 3343. (b) Schubert, U.; Hüsing, N.; Lorenz, A. *Chem. Mater.* **1995**, *7*, 2010.

(4) Selected references on the single-source precursor approach: (a) Cowley, A. H.; Jones, R. A. *Angew. Chem., Int. Ed. Engl.* **1989**, *28*, 1208. (b) Apblett, A. W.; Warren, A. C.; Barron, A. R. *Chem. Mater.* **1992**, *4*, 167. (c) Chaput, F.; Lecomte, A.; Dauger, A.; Boilot, J. P. *Chem. Mater.* **1989**, *1*, 199. (d) Hubert-Pfalzgraf. L. G. *New J. Chem.* **1987**, *11*, 663. (e) Mehrotra, R. C. *J. Non-Cryst. Solids* **1990**, *121*, 1. (f) Bradley, D. C. *Polyhedron* **1994**, *13*, 1111. (g) Chandler, C. D.; Roger, C.; Hampden-Smith, M. J. *Chem. Rev.* **1993**, *93*, 1205. (h) Narula, C. K.; Varshney, A.; Riaz, U. *Chem. Vap. Deposition* **1996**, *2*, 13. (i) Altherr, A.; Wolfganger, H.; Veith, M. *Chem. Vap. Deposition* **1999**, *5*, 87.

10.1021/cm010027x CCC: $20.00

Over the past decade we have been investigating the structure, bonding, and reactivity of transition-metal and main-group element tris(*tert*-butoxy)siloxy complexes of the type M[OSi(O^{t}Bu)$_3$]$_n$.[5−19] These well-defined, oxygen-rich compounds can be used as convenient precursors to amorphous, homogeneous, metal oxide−silica or metal silicate materials. The thermolytic conversions of these complexes to mixed-element oxide materials occur cleanly, at relatively low temperatures (typically below 200 °C), via the elimination of isobutene and water. The solution thermolyses of these precursors in nonpolar media lead to the formation of gels, which provide high surface area xerogels upon conventional drying, or aerogels using supercritical drying techniques. We have employed this *thermolytic molecular precursor* method for the low-temperature synthesis of a variety of homogeneous metal−silicon−oxide materials with interesting and sometimes unique properties.[5−19] Other groups have developed nonhydrolytic routes to mixed-element oxides based on molecular solution chemistry. These methods include the condensation of metal alkoxides with metal acetates[20] or metal halides.[21]

Oxide-supported (e.g., silica, alumina, and zirconia) chromium catalysts are used in the commercial polymerization of ethylene[22] and in the dehydrogenation of light paraffins.[23] We have been interested in the development of chromium complexes based on the tris(*tert*-butoxy)siloxy ligand for use as molecular precursors to Cr/Si/O materials and also as models for heterogeneous chromium catalysts. Silica-supported alkyl chromium(IV) species,[24] oxo alkyls of Cr(IV) and Cr(V),[25] a bimetallic chromium(VI) siloxane complex,[26] and chromium-containing polyhedral oligometallasilasesquioxanes[27] are examples of compounds that have been used in model studies for reactions catalyzed by chromium−silicon−oxide catalysts.

Previously, we reported the Cr(II) and Cr(III) complexes Cr[OSi(O^{t}Bu)$_3$]$_2$(NHEt$_2$)$_2$ and Cr[OSi(O^{t}Bu)$_3$]$_3$(NHEt$_2$)$_2$, which were isolated in low to moderate yields from the reaction of Cr(NEt$_2$)$_4$ and 4 equiv of HOSi(O^{t}Bu)$_3$.[9] No Cr(IV) complexes were isolated or observed from this reaction. Anionic species with the molecular formula MCr[OSi(O^{t}Bu)$_3$]$_4$ (M = Na or K) have also been isolated and characterized.[28] The Cr(IV) tris(alkyl)siloxide Cr(OSiEt$_3$)$_4$ was synthesized by Bradley et al. via the silanolysis of Cr(O^{t}Bu)$_4$ with 4 equiv of HOSiEt$_3$.[29] The analogous reactions using 4 equiv of tris(*tert*-butoxy)silanol previously resulted in the observation of only reduced chromium products.[9] Here, we report the syntheses of (^{t}BuO)$_3$CrOSi(O^{t}Bu)$_3$ (**1**) and (^{t}BuO)$_2$Cr[OSi(O^{t}Bu)$_3$]$_2$ (**2**) via the silanolysis of Cr(O^{t}Bu)$_4$ with tris(*tert*-butoxy)silanol. The thermolytic conversions of **1** to chromia−silica materials under two sets of conditions were examined, and the resulting materials were studied as catalysts for the oxidative dehydrogenation of propane to propene.

Results and Discussion

Tris(*tert*-butoxy)siloxychromium(IV) Complexes. The reaction of 1 equiv of HOSi(O^{t}Bu)$_3$ with Cr(O^{t}Bu)$_4$ in the absence of solvent at 80 °C for 30 min under flowing nitrogen afforded the Cr(IV) alkoxysiloxy complex (^{t}BuO)$_3$CrOSi(O^{t}Bu)$_3$ (**1**, eq 1). The air- and moisture-sensitive blue solid present after removal of the volatile materials was purified by sublimation at 80 °C under reduced pressure (82% yield). Subsequent recrystallization from a mixture of toluene and acetonitrile (1:1) at −30 °C gave analytically pure, blue, platelike crystals in a yield of 61%. Alternatively, the blue solid residue that remains after removal of the volatile impurities can be recrystallized directly from a mixture of toluene and acetonitrile (1:1) to give analytically pure **1** in isolated yields consistently greater than 80%. A small amount of an unknown volatile blue-green liquid, possibly a reduced chromium alkoxide, is also produced in this reaction but was not isolated or characterized. The use of organic solvents reduced the yield of **1** and increased the reaction time significantly (to >12 h).

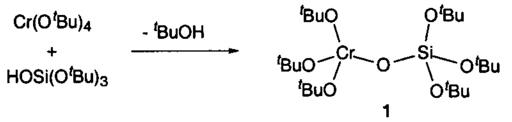

(1)

---

(5) McMullen, A. K.; Tilley, T. D.; Rheingold, A. L.; Geib, S. J. *Inorg. Chem.* **1989**, *28*, 3772.

(6) McMullen, A. K.; Tilley, T. D.; Rheingold, A. L.; Geib, S. J. *Inorg. Chem.* **1990**, *29*, 2228.

(7) Terry, K. W.; Tilley, T. D. *Chem. Mater.* **1991**, *3*, 1001.

(8) Terry, K. W.; Gantzel, P. K.; Tilley, T. D. *Chem. Mater.* **1992**, *4*, 1290.

(9) Terry, K. W.; Gantzel, P. K.; Tilley, T. D. *Inorg. Chem.* **1993**, *32*, 5402.

(10) Terry, K. W.; Lugmair, C. G.; Gantzel, P. K.; Tilley, T. D. *Chem. Mater.* **1996**, *8*, 274.

(11) Su, K.; Tilley, T. D.; Sailor, M. J. *J. Am. Chem. Soc.* **1996**, *118*, 3459.

(12) Su, K.; Tilley, T. D. *Chem. Mater.* **1997**, *9*, 588.

(13) Terry, K. W.; Lugmair, C. G.; Tilley, T. D. *J. Am. Chem. Soc.* **1997**, *119*, 9745.

(14) Rulkens, R.; Tilley, T. D. *J. Am. Chem. Soc.* **1998**, *120*, 9959.

(15) Lugmair, C. G.; Tilley, T. D. *Inorg. Chem.* **1998**, *37*, 764.

(16) Terry, K. W.; Su, K.; Tilley, T. D.; Rheingold, A. L. *Polyhedron* **1998**, *17*, 891.

(17) Rulkens, R. R.; Male, J. L.; Terry, K. W.; Olthof, B.; Khodakov, A.; Bell, A. T.; Iglesia, E.; Tilley, T. D. *Chem. Mater.* **1999**, *11*, 2966.

(18) Coles, M. P.; Lugmair, C. G.; Terry, K. W.; Tilley, T. D. *Chem. Mater.* **2000**, *12*, 122.

(19) Male, J. L.; Niessen, H. G.; Bell, A. T.; Tilley, T. D. *J. Catal.* **2000**, *194*, 431.

(20) Jansen, M.; Guenther, E. *Chem. Mater.* **1995**, *7*, 2110.

(21) Vioux, A. *Chem. Mater.* **1997**, *9*, 2292.

(22) (a) Clark, A. *Catal. Rev.* **1970**, *3*, 145. (b) Karol, F. J.; Karapinka, G. L.; Wu, C.; Dow, A. W.; Johnson, R. N.; Carrick, W. L. *J. Polym. Sci., Part A-1* **1972**, *10*, 2621. (c) McDaniel, M. P.; Leigh, C. H.; Wharry, S. M. *J. Catal.* **1989**, *120*, 170. (d) Karol, F. J. *Catal. Rev.-Sci. Eng.* **1984**, *26*, 557. (e) Badayal, J. P. S.; Ruddick, V. J. *J. Phys. Chem. B* **1998**, *102*, 2991.

(23) For recent examples see: (a) Derossi, S.; Ferraris, G.; Fremiotti, S.; Garrone, E.; Ghiotti, G.; Campa, M. C.; Indovina, V. *J. Catal.* **1994**, *148*, 36. (b) Chang, W. C.; Mimura, N.; Saito, M.; Takahara, I. *Catal. Today* **1998**, *45*, 55. (c) De Rossi, S.; Casaletto, M. P.; Ferraris, G.; Cimino, A.; Minelli, G. *Appl. Catal. A* **1998**, *167*, 257. (d) Gorriz, O. F.; Cadus, L. E. *Appl. Catal. A* **1999**, *180*, 247. (e) Sloczynski, J.; Grzybowska, B.; Grabowski, R.; Kozlowska, A.; Wcislo, K. *Phys. Chem. Chem. Phys.* **1999**, *1*, 333. (f) Alcántara-Rodríguez, M.; Rodríguez-Castellón, E.; Jiménez-López, A. *Langmuir* **1999**, *15*, 1115. (g) Pérez-Reina, F. J.; Rodríguez-Castellón, E.; Jiménez-López, A. *Langmuir* **1999**, *15*, 8421. (h) Weckhuysen, B. M.; Schoonheydt, R. A. *Catal. Today* **1999**, *51*, 223.

(24) Nait, J. A.; Paquet, V.; Scott, S. L. *J. Am. Chem. Soc.* **1998**, *120*, 415.

(25) Noh, S. K.; Heintz, R. A.; Haggerty, B. S.; Rheingold, A. L.; Theopold, K. H. *J. Am. Chem. Soc.* **1992**, *114*, 1892.

(26) Abbenhuis, H. C. L.; Vorstenbosch, M. L. W.; van Santen, R. A.; Smeets, W. J. J.; Spek, A. L. *Inorg. Chem.* **1997**, *36*, 6432.

(27) (a) Blanski, R. L.; Feher, F. J. *J. Chem. Soc., Chem. Commun.* **1990**, 1614. (b) Feher, F. J.; Walzer, J. F. *Inorg. Chem.* **1990**, *29*, 1604.

(28) Terry, K. W. Ph.D. Thesis, University of California at San Diego, San Diego, CA, 1993.

(29) Alyea, E. C.; Basi, J. S.; Bradley, D. C.; Chisholm, M. H. *J. Chem. Soc. A* **1971**, 772.

Table 1. Selected Bond Distances (Å) and Angles (deg) for 1[a]

		Distances			
Cr(1)−O(1)	1.670(5)	Si(1)−O(1)	1.643(5)	O(6)−C(17)	1.444(9)
Cr(1)−O(5)	1.678(5)	Si(1)−O(2)	1.662(6)	O(7)−C(21)	1.376(9)
Cr(1)−O(6)	1.690(6)	Si(1)−O(3)	1.654(6)	O(5)−C(13)	1.428(9)
Cr(1)−O(7)	1.646(6)	Si(1)−O(4)	1.687(5)	O(3)−C(5)	1.429(9)
O(4)−C(9)	1.432(8)	O(2)−C(1)	1.401(10)		
		Angles			
O(1)−Cr(1)−O(5)	109.6(3)	O(1)−Si(1)−O(2)	112.1(3)	Cr(1)−O(1)−Si(1)	151.2(4)
O(1)−Cr(1)−O(7)	108.3(3)	O(1)−Si(1)−O(3)	111.1(4)	Cr(1)−O(5)−C(13)	131.8(5)
O(1)−Cr(1)−O(6)	113.6(3)	O(1)−Si(1)−O(4)	110.8(3)	Cr(1)−O(6)−C(17)	131.6(5)
O(5)−Cr(1)−O(7)	111.3(3)	O(2)−Si(1)−O(3)	108.8(3)	Cr(1)−O(7)−C(21)	139.4(6)
O(5)−Cr(1)−O(6)	105.1(3)	O(2)−Si(1)−O(4)	106.4(3)	Si(1)−O(2)−C(1)	139.4(6)
O(6)−Cr(1)−O(7)	109.0(3)	O(3)−Si(1)−O(4)	107.6(3)	Si(1)−O(3)−C(5)	135.1(5)
Si(1)−O(4)−C(9)	131.4(5)				

[a] These values are averaged due to the heavy-atom disorder (see text) and should be treated with caution.

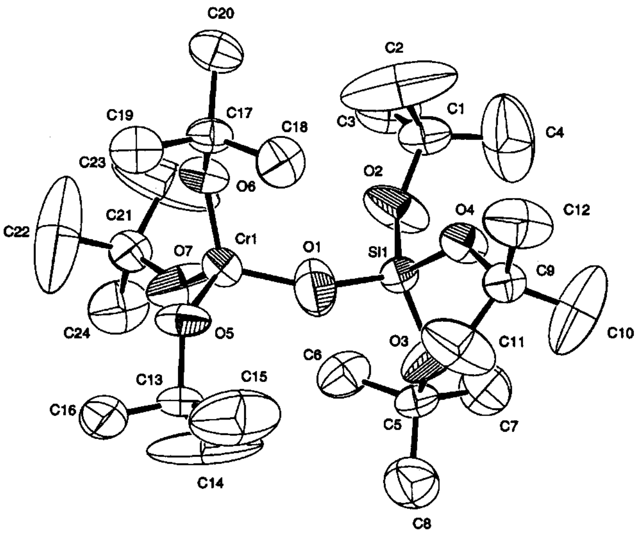

Figure 1. ORTEP diagram of $(^tBuO)_3CrOSi(O^tBu)_3$ (**1**) with 50% thermal ellipsoids. Hydrogen atoms have been omitted for clarity.

Table 2. Crystallographic Data for 1 and 2

	1	2
formula	$CrSiC_{24}O_7H_{54}$	$CrSi_2C_{32}O_{10}H_{72}$
crystal system	monoclinic	monoclinic
space group	$P2_1/n$	$P2_1/n$
Z	4	4
cell constants		
a (Å)	9.7114(6)	9.6853(3)
b (Å)	16.3103(10)	16.6023(5)
c (Å)	20.5148(10)	27.2800(9)
β (deg)	95.943(2)	97.264(1)
V (Å^3)	3232.0(3)	4351.4(2)
D_{calc} (g/cm^3)	1.099	1.107
F_{000}	1168.00	1584.00
μ(Mo Kα) (cm^{-1})	18.09	17.60
radiation	Mo Kα ($\lambda = 0.71073$ Å)	Mo Kα ($\lambda = 0.71073$ Å)
$2\theta_{max}$ (deg)	41.6	49.4
scan type	ω (0.3° per frame)	ω (0.3° per frame)
measured reflections	10685	20291
unique reflections	3649	7547
$R(F)$; $R_w(F)$; $R_{all}(F)$	0.054; 0.056; 0.118	0.046; 0.045; 0.141
GOF indicator	1.94	1.48

A magnetic susceptibility study of **1** from 5 to 200 K revealed Curie−Weiss behavior ($\theta = -1.26$ K) and gave an average value of $\mu_{eff} = 2.80\ \mu_B$, indicating the presence of two unpaired electrons (spin only value for a d^2 system is 2.83 μ_B). For comparison, the chromium starting material $Cr(O^tBu)_4$ has a magnetic moment of $\mu_{eff} = 2.80\ \mu_B$ (98−298 K)[29] and the value determined in solution at room temperature was 2.86 μ_B (Evans method).[30] The ^{1}H NMR spectrum of **1** contains two broad resonances in a 1:1 ratio, centered at ~3.4 and ~1.7 ppm, corresponding to the $Cr(O^tBu)_3$ and $Si(O^tBu)_3$ groups, respectively. The ^{1}H NMR spectrum of $Cr(O^tBu)_4$ (benzene-d_6) exhibits one broad resonance at ~3 ppm, which is remarkably close to the chemical shift expected for diamagnetic O^tBu protons.[30] The parent ion of **1** (m/z 534) was observed by fast atom bombardment mass spectrometric analysis (FAB-MS).

The molecular structure of **1** is shown in Figure 1, selected bond distances and angles are given in Table 1, and the crystallographic data are listed in Table 2. Crystals of **1** generally diffracted poorly, and therefore the structure was determined only to a resolution of 1.0 Å. The geometries about the Cr and Si centers are quite similar and could not be distinguished in the refinement. As a result of this disorder, the bond distances and angles are average values and should be viewed with caution. However, it is clear that this d^2 complex exhibits a pseudo-tetrahedral coordination geometry at the chromium center.

The reaction of 2 equiv of $HOSi(O^tBu)_3$ with $Cr(O^tBu)_4$ as a solvent-free mixture at 80 °C afforded $(^tBuO)_2Cr[OSi(O^tBu)_3]_2$ (**2**, eq 2) in highly variable isolated yields (0−68%). The blue-green air- and moisture-sensitive solid was purified by recrystallization from a mixture of toluene and acetonitrile (1:1) at −30 °C.

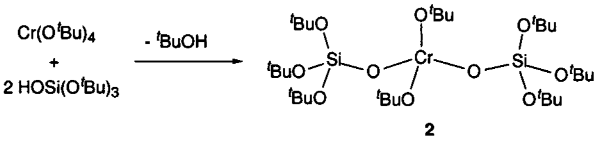

(2)

2

A magnetic susceptibility study of **2** (5−200 K) provided an average value of $\mu_{eff} = 2.71\ \mu_B$, indicating two unpaired electrons. Complex **2** obeys the Curie−Weiss law over this temperature range, with $\theta = -2.76$ K. The ^{1}H NMR spectrum of **2** contains two broad resonances centered at ~3.4 and ~1.7 ppm, corresponding to the CrO^tBu and $OSi(O^tBu)_3$ groups, respectively. The parent ion (m/z 724) was observed by FAB-MS analysis.

The molecular structure of **2** is shown in Figure 2 and selected bond distances and angles are given in Table

---

(30) Thaler, E. G.; Rypdal, K.; Haaland, A.; Caulton, K. G. *Inorg. Chem.* **1989**, *28*, 2431.

Table 3. Selected Bond Distances (Å) and Angles (deg) for 2

Distances					
Cr(1)−O(1)	1.744(3)	Si(1)−O(3)	1.612(3)	Si(2)−O(7)	1.444(9)
Cr(1)−O(2)	1.739(3)	Si(1)−O(4)	1.611(4)	Si(2)−O(8)	1.376(9)
Cr(1)−O(3)	1.763(3)	Si(1)−O(5)	1.614(3)	Si(2)−O(9)	1.428(9)
Cr(1)−O(7)	1.749(3)	Si(1)−O(6)	1.612(3)	Si(2)−O(10)	1.429(9)
O(1)−C(1)	1.432(5)	O(6)−C(17)	1.439(5)	O(10)−C(29)	1.464(6)
O(2)−C(5)	1.432(5)	O(8)−C(21)	1.439(5)	O(5)−C(13)	1.433(5)
O(4)−C(9)	1.443(6)	O(9)−C(25)	1.441(5)		
Angles					
O(1)−Cr(1)−O(2)	106.24(16)	O(3)−Si(1)−O(4)	111.36(18)	O(7)−Si(2)−O(8)	110.08(17)
O(1)−Cr(1)−O(3)	104.87(17)	O(3)−Si(1)−O(5)	110.71(18)	O(7)−Si(2)−O(9)	106.00(17)
O(1)−Cr(1)−O(7)	108.84(16)	O(3)−Si(1)−O(6)	106.96(18)	O(7)−Si(2)−O(10)	112.97(18)
O(2)−Cr(1)−O(3)	113.72(16)	O(4)−Si(1)−O(5)	106.5(2)	O(8)−Si(2)−O(9)	113.62(17)
O(2)−Cr(1)−O(7)	111.66(15)	O(4)−Si(1)−O(6)	107.3(2)	O(8)−Si(2)−O(10)	107.06(17)
O(3)−Cr(1)−O(7)	111.06(15)	O(5)−Si(1)−O(6)	113.99(17)	O(9)−Si(2)−O(10)	107.20(17)
Cr(1)−O(1)−C(1)	132.2(3)	Cr(1)−O(2)−C(5)	133.7(3)	Cr(1)−O(3)−Si(1)	145.2(2)
Cr(1)−O(7)−Si(2)	156.9(2)	Si(1)−O(4)−C(9)	131.4(3)	Si(1)−O(5)−C(13)	134.3(3)
Si(1)−O(6)−C(17)	132.0(3)	Si(2)−O(8)−C(21)	132.4(3)	Si(2)−O(9)−C(25)	131.2(3)
Si(2)−O(10)−C(29)	131.3(3)				

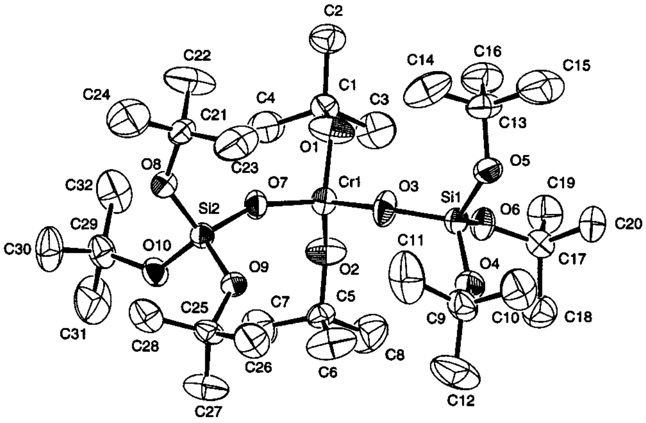

Figure 2. ORTEP diagram of $(^tBuO)_2Cr[OSi(O^tBu)_3]_2$ (**2**) with 50% thermal ellipsoids. Hydrogen atoms have been omitted for clarity.

3. Crystals of **2** diffracted well and did not contain disorder in the Cr and Si atom positions. Complex **2** exhibits a pseudo-tetrahedral coordination geometry at chromium, with a mean Cr−O distance of 1.754(3) Å. For comparison, the gas-phase electron diffraction structure of $Cr(O^tBu)_4$ features a Cr−O bond distance of 1.751(7) Å.[30] In addition, the Cr(IV) alkoxide $Cr[OCH(CMe_2)_2]_4$ exhibits an average Cr−O distance of 1.773(3) Å.[31] In general, comparable distances and angles in **1** and **2** appear to be quite similar.

When solvents (toluene, pentane, THF, Et_2O, and C_6H_6) were employed in carrying out the reaction of eq 2, complex product mixtures were obtained. In addition, the reaction of **1** with 1 equiv of $HOSi(O^tBu)_3$ did not prove to be a viable route to pure **2**. These problems may arise from competing electron-transfer reactions, which have been shown by Caulton et al. to be a dominant reaction pathway for $Cr(O^tBu)_4$.[30] In fact, numerous attempts to convert **1** to **2** resulted in green materials, which may arise from the presence of reduced Cr species. Attempted syntheses of $(^tBuO)Cr[OSi(O^tBu)_3]_3$ and $Cr[OSi(O^tBu)_3]_4$ using 3 and 4 equiv of $HOSi(O^tBu)_3$ gave either intractable mixtures or **2** as the only isolated product in very low yield. Thus, the previous suggestion that $Cr[OSi(O^tBu)_3]_4$ may be unstable[9] seems to be supported by these results.

Table 4. Products from the Hydrolyses of 1 and 2[a]

	1	2
product	obsvd (theor)	obsvd (theor)
^tBuOH	3.0 (3)	2.5 (2)
$HOSi(O^tBu)_3$	1.0 (1)	2.0 (2)

[a] Equivalents based on the amount of **1** or **2** used.

Hydrolyses of 1 and 2. Samples of **1** or **2** and a ferrocene standard were dissolved in benzene-d_6 and hydrolyzed by the addition of 5 μL of H_2O via a syringe. The hydrolysis products, identified by ^1H NMR spectroscopy, were the expected amounts of *tert*-butyl alcohol and tris(*tert*-butoxy)silanol (Table 4). The insoluble brown powder formed after the hydrolysis of each complex was calcined at 1200 °C in O_2 and subsequently analyzed by powder X-ray diffraction (PXRD) at room temperature. The only reflections observed in both cases were due to the presence of crystalline Cr_2O_3.

The results of these hydrolysis studies clearly indicate that a hydrolytic sol−gel route to homogeneous Cr/Si/O materials using either **1** or **2** would be adversely complicated by cleavage of the Cr−O−Si linkage early in the gelation process. Thus, further attempts to obtain Cr/Si/O materials from **1** and **2** were based on the thermolytic molecular precursor method.[5−19]

Solid-State Thermolyses of 1 and 2. The solid-state thermolytic conversions of **1** and **2** to ceramic materials under an inert atmosphere (Ar or N_2) were examined. Both **1** and **2** thermally decompose at low temperature, as demonstrated by thermogravimetric analysis (TGA). The TGA traces for **1** and **2** under an atmosphere of argon are shown in Figures 3 and 4, respectively. The differential thermal analysis (DTA) curve for **1** revealed a sharp endothermic transition from 108 to 110 °C just prior to the major decomposition endotherm and precipitous mass loss. This initial endothermic transition presumably corresponds to a melt; however, decomposition of this complex at about the same temperature precluded visual confirmation of the melting behavior. No such initial endothermic transition was observed for **2** prior to decomposition. The onset temperatures for the thermal decompositions of **1** and **2** are approximately 100 and 90 °C, respectively, with precipitous weight loss initiating at ca. 140 °C. Thus, both complexes thermolytically transform at remarkably low temperature.[13] For the decomposition of **1** under Ar,

---

(31) Bochmann, M.; Wilkinson, G.; Yang, G. B.; Hursthouse, M. B.; Malik, K. M. *J. Chem. Soc., Dalton Trans.* **1980**, 1863.

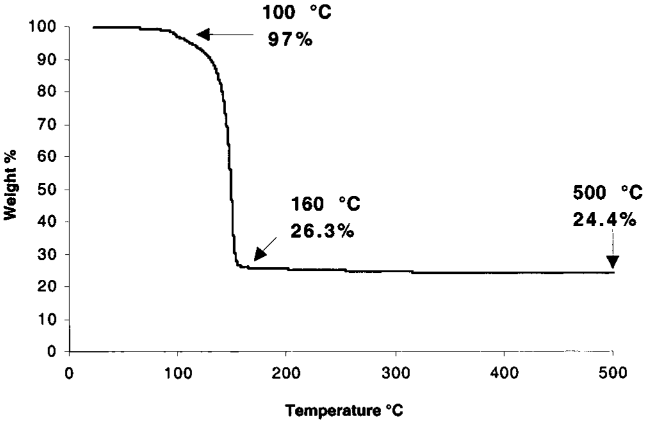

Figure 3. TGA trace for **1** under a flow of argon (100 cm^3/min) with a heating rate of 10 °C/min.

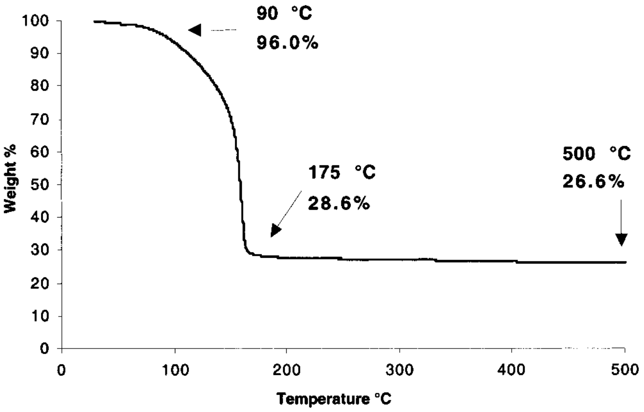

Figure 4. TGA trace for **2** under a flow of argon (100 cm^3/min) with a heating rate of 10 °C/min.

the ceramic yield of 24.4% is close to that expected for formation of $CrO_{1.5}$·SiO_2 (25.4%). For comparison, the calculated yields for CrO_2·SiO_2 and CrO_3·SiO_2 are 26.9% and 29.9%, respectively. The ceramic yield for the thermal decomposition of **2** under flowing argon was 26.6%, which is in good agreement with the theoretical yield for $CrO_{1.5}$·$2SiO_2$ (27.1%). On the basis of the stoichiometry of **2**, the calculated ceramic yield for CrO_2·$2SiO_2$ is 28.2% and that for CrO_3·$2SiO_2$ is 30.4%. These ceramic yields suggest that the main Cr species present in each material at elevated temperatures is the thermodynamically favored chromium oxide Cr_2O_3. Indeed, particles of Cr_2O_3 are often observed, even at low Cr loadings, on silica surfaces, and the amount of Cr_2O_3 formed increases with Cr loading and calcination temperature.[32]

The high synthetic yields and ease of purification of **1** prompted us to further study its use as a single-source molecular precursor to Cr/Si/O materials. Large-scale solid-state thermolyses of **1** were conducted by heating Schlenk tubes containing the precursor complex under a flow of N_2 at 180 °C. The ceramic material **CrOSi$_{ss}$**, obtained from the solid-state thermal decomposition of **1**, was ground to a fine powder and calcined at various temperatures. Monitoring the crystallization behavior of **CrOSi$_{ss}$** by PXRD analysis revealed that the material remained amorphous until 600 °C, at which time very weak reflections due to the presence of crystalline Cr_2O_3 were evident (Figure 5). Further calcinations of **CrOSi$_{ss}$** (up to 1200 °C) led to phase separation and increased crystallization of Cr_2O_3.

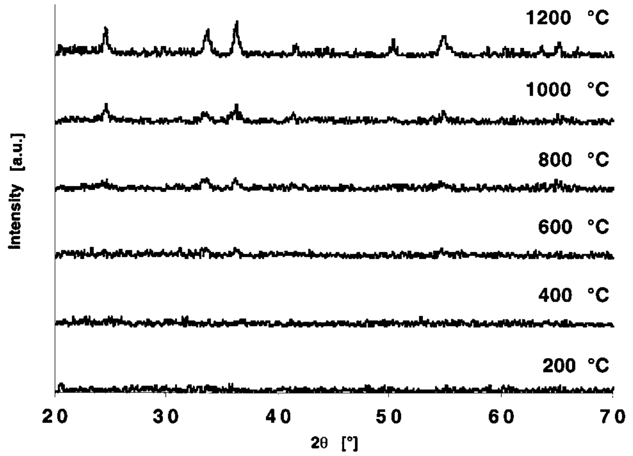

Figure 5. Room-temperature PXRD patterns of **CrOSi$_{ss}$** after calcination at various temperatures under flowing oxygen (100 cm^3/min).

Table 5. Properties of the Materials Derived from 1[a]

calcination temp (°C)	BET surface area (m^2/g)	total pore volume (cm^3/g)	micropore area (m^2/g)	mesopore area (m^2/g)
		CrOSi$_{xg}$		
uncalcined	315	0.31	175	135
400	180	0.21	60	120
500	205	0.20	110	95
		CrOSi$_{ss}$		
uncalcined	315	0.20	230	85
400	275	0.17	160	115
500	275	0.18	140	135

[a] All surface areas are to the nearest 5 m^2/g to reflect the error in measurement.

Surface area measurements of **CrOSi$_{ss}$**, after calcination at various temperatures, were obtained by means of the Brunauer–Emmett–Teller N_2 adsorption–desorption method (BET).[33] Pore size distributions were analyzed by the Barrett–Joyner–Halenda (BJH) method[34] and the micropore areas were determined by t-plot methods (Table 5).[35] The nitrogen adsorption–desorption isotherm (Figure 6) for **CrOSi$_{ss}$**, after calcination at 500 °C, closely resembles that expected for a type IV isotherm and displays type H2 hysteresis.[36] This type of hysteresis has been attributed to the presence of ink-bottle-shaped mesopores; however, it is now recognized that this geometric model may be an oversimplification.[36] Uncalcined **CrOSi$_{ss}$** had a remarkably high surface area of 315 m^2/g and a relatively small pore volume of 0.21 cm^3/g. This surface area is higher than those typically observed for solid-phase transformations using other alkoxysiloxy-based precursors[7,8,13] and presumably results from the nature of the molecular packing in the solid phase of the complex. For comparison, the surface area of the material generated via the solid-state thermolysis of $Zr[OSi(O^tBu)_3]_4$ was 120 m^2/g

---

[32] Weckhuysen, B. M.; Wachs, I. E.; Schoonheydt, R. A. *Chem. Rev.* **1996**, *96*, 3327.

[33] Brunauer, S.; Emmett, P. H.; Teller, E. *J. Am. Chem. Soc.* **1938**, *60*, 309.

[34] Barrett, E. P.; Joyner, L. G.; Hakebda, P. P. *J. Am. Chem. Soc.* **1951**, *73*, 373.

[35] Lippens, B. C.; de Boer, J. H. *J. Catal.* **1965**, *4*, 319.

[36] Sing, K. S. W.; Everett, D. H.; Haul, R. A.; Moscou, L.; Pierotti, R. A.; Rouquerol, J.; Siemieniewska, T. *Pure Appl. Chem.* **1985**, *57*, 603.

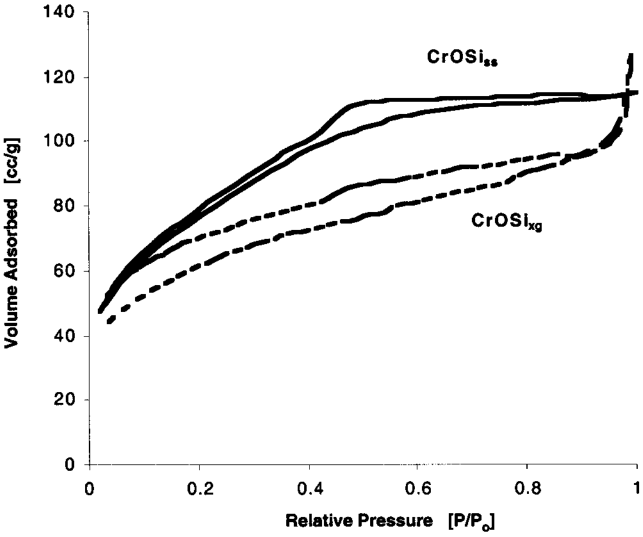

Figure 6. Adsorption−desorption isotherms for the materials derived from **1**.

(pore volume 0.84 cm^3/g),[13] and the surface areas of the materials generated from the solid-state conversions of $\{Me_2Al[\mu\text{-}OSi(O^tBu)_3]\}_2$ and $[Me(O^tBu)AlOSi(O^tBu)_3]_3$ were 30 and 270 m^2/g, respectively.[8] The surface area of **CrOSi$_{ss}$** was only reduced to 275 m^2/g after calcination at 500 °C (pore volume 0.18 cm^3/g). The micropore contribution to the total surface area decreases with increasing calcination temperature, as indicated from the t-plot analyses. The BJH pore size distribution for **CrOSi$_{ss}$** indicated that the majority of the pores had radii less than 10 Å.

Transmission electron micrographs of **CrOSi$_{ss}$**, after calcination at 200 °C, revealed clumps of primary particles of various sizes (Figure 7). Elemental analysis of this material gave a Cr:Si ratio of 1:1.02, indicating clean conversion of the molecular precursor with retention of the stoichiometry. Elemental analysis also revealed that the carbon and hydrogen contents of **CrOSi$_{ss}$** were quite low after calcination at 200 °C (3.85 and 1.7%, respectively), and after calcination at 500 °C no carbon was detected (<0.2%) and the hydrogen content was 0.24%.

Xerogel Formation from 1. Complex **1** was also examined in solution-phase thermolytic molecular precursor routes to bulk mixed-element oxide xerogels. The thermal decomposition of *n*-octane solutions of **1** (0.1 M) at 180 °C over 24 h led to the formation of light green gelatinous precipitates that, upon slow air-drying over 3 days, afforded xerogels **CrOSi$_{xg}$**, in ceramic yields of ca. 29%. Thermogravimetric analyses of these air-dried gels revealed further weight losses of up to 19% through 1200 °C, attributed to dehydration and condensation of the network as well as removal of residual ^{t}BuOH, *n*-octane, and H_2O. A representative TGA trace for **CrOSi$_{xg}$** under O_2 is shown in Figure 8. Interestingly, the material changed color from light green to brown at ca. 400 °C, coincident with a sharp mass loss of 9.4%. The brown color persisted until ca. 500 °C when the powder became green, coincident with the beginning of a gradual weight loss of 5.7%. The green color, associated with nanocrystalline Cr_2O_3, continuously intensified until 1200 °C. Differential thermal analysis revealed a broad exothermic transition centered around 275 °C in the DTA trace. This exotherm was coincident with the 9.4% mass loss and indicates a compositional change.

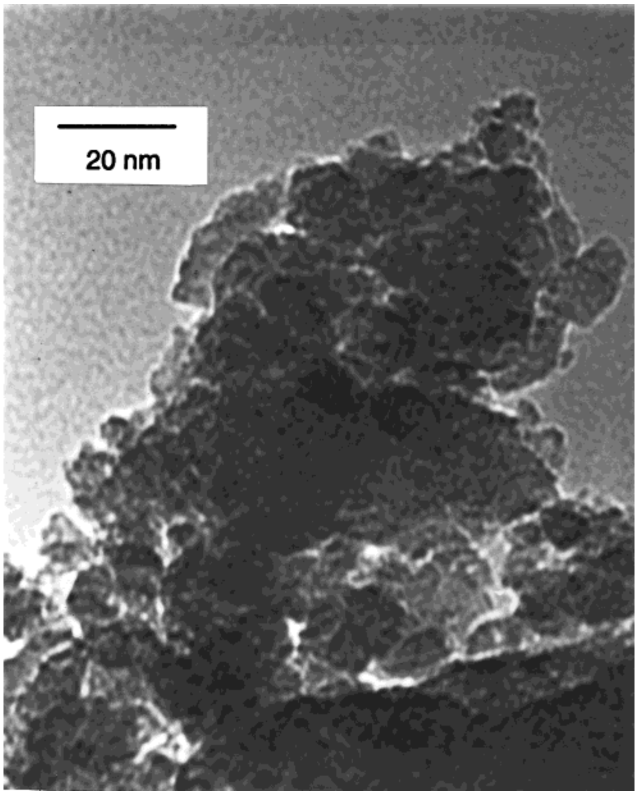

Figure 7. TEM image of **CrOSi$_{ss}$** after calcination at 200 °C under flowing oxygen.

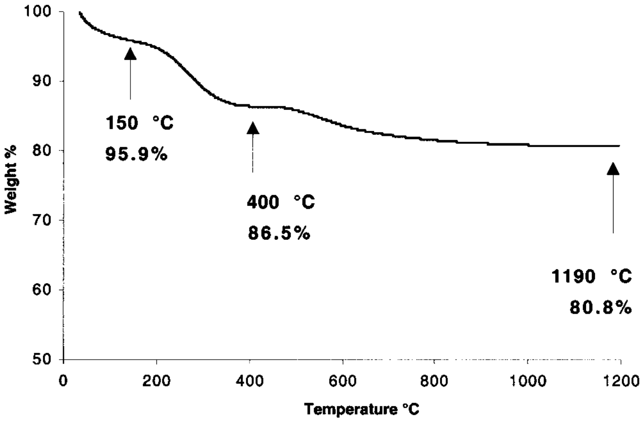

Figure 8. TGA trace of **CrOSi$_{xg}$** under a flow of oxygen (100 cm^3/min) with a heating rate of 10 °C/min.

The chemical transformations associated with the conversions of **1** and **2** to chromia−silica materials in benzene-d_6 solution were studied by ^{1}H NMR spectroscopy. A sample of the molecular precursor was dissolved in benzene-d_6 along with a ferrocene standard and sealed in an NMR tube after three freeze−pump−thaw cycles. The tube was then heated to 180 °C for about 1 h, until the solution had changed from blue to colorless with the formation of a precipitate. The soluble decomposition products were determined to be isobutene, *tert*-butyl alcohol, and water (Table 6). The lower than expected amount of water may be attributed to the low solubility of water in benzene and/or the presence of an oxide desiccant formed during the thermolysis. The

Table 6. Decomposition Products from the Solution Thermolyses of 1 and 2[a]

	1	2
product	obsvd (theor)	obsvd (theor)
$CH_2{=}CMe_2$	5.0 (6)	7.5 (8)
H_2O	0.5 (3)	1.0 (4)
^tBuOH	0.1 (0)	1.0 (0)
$HOSi(O^tBu)_3$	0 (0)	0 (0)

[a] Equivalents based on the amount of **1** or **2** used.

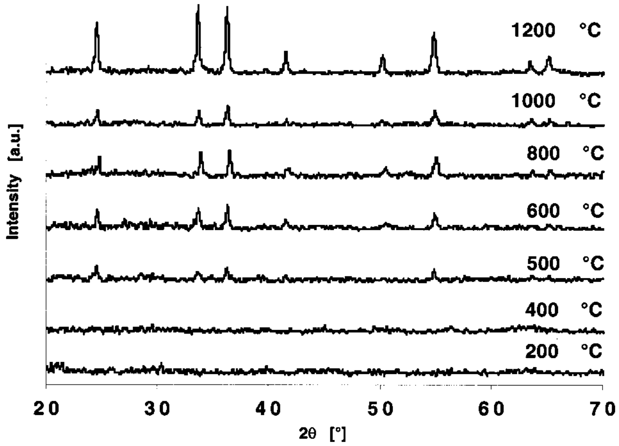

Figure 9. Room-temperature PXRD patterns of **CrOSi$_{xg}$** after calcination under a flow of oxygen (100 cm^3/min) at various temperatures.

small amount of ^{t}BuOH observed may be due to hydrolysis of precursor species by water as it forms in the reaction. However, note that HOSi(O^{t}Bu)$_3$ (a potential hydrolysis product) was not observed in either transformation. A portion of the isobutene is assumed to be present in the gas phase above the deuterated solvent, thus preventing detection of the expected stoichiometric amounts.

Calcination of **CrOSi$_{xg}$**, as a finely ground powder, was monitored by room-temperature PXRD analysis (Figure 9). Weak reflections for crystalline Cr_2O_3 were observed in the material calcined at 500 °C. As the calcination temperature was increased, the crystallization of Cr_2O_3 continued, as indicated by increased reflection intensities. The lower temperature at which Cr_2O_3 crystallizes in **CrOSi$_{xg}$** (vs **CrOSi$_{ss}$**) suggests that the xerogel may not be as atomically well-mixed. This was also suggested by a comparison of the IR spectra of the calcined samples of **CrOSi$_{xg}$** and **CrOSi$_{ss}$**, which showed that the appearance of bands at ca. 630, 570, and 470 cm^{-1} (attributed to crystalline Cr_2O_3 by comparison to an authentic sample) occurred earlier for **CrOSi$_{xg}$**, and this material exhibited increased intensities for these bands (relative to those for **CrOSi$_{ss}$**) up to 1000 °C. After calcination at 1200 °C the two materials exhibited IR spectra that were quite similar, indicating that a similar amount of Cr_2O_3 was present. Attempts to obtain Raman spectra of these materials were complicated, presumably by fluorescence, resulting from the high Cr content.[37]

Transmission electron micrographs of **CrOSi$_{xg}$** after O_2 calcinations at 200 and 1200 °C are shown in Figures 10 and 11, respectively. The micrograph of the xerogel calcined at 200 °C shows what appears to be a regular pattern of similarly sized nanoparticles. In contrast to this, a wide size distribution of approximately rectangular Cr_2O_3 crystallites are evident in the micrograph of **CrOSi$_{xg}$** calcined at 1200 °C. This representative micrograph illustrates that the Cr_2O_3 nanocrystals range in size from ca. 2 × 6 nm to larger than ca. 40 × 60 nm.

Surface area and pore volume data for the **CrOSi$_{xg}$** materials are given in Table 5. The nitrogen adsorption–desorption isotherm for the xerogel (Figure 6) has characteristics that approximate those of type I for the lower relative pressure region, but at high relative pressure (approaching $P/P_0 = 1$) the isotherm appears to have type II character.[36] The hysteresis present in the isotherm appears to approximate that of type H4, which has been associated with narrow slitlike pores in microporous materials.[36] Increases in adsorbed volume of nitrogen at high relative pressure in mesoporous silica materials have been attributed to textural mesoporosity between particles.[38] Thus, the data for **CrOSi$_{xg}$** suggest the presence of both micoporosity and textural mesoporosity resulting from interparticle packing. BJH pore size distributions indicated that the majority of the pores had radii less than 10 Å.

Uncalcined **CrOSi$_{xg}$** had a surface area of 315 m^2/g, which is about the same as that obtained for **CrOSi$_{ss}$**. For comparison, the surface area of **CrOSi$_{xg}$** is lower than that observed for the xerogel generated via the solution thermolysis of Zr[OSi(O^{t}Bu)$_3$]$_4$ (ca. 700 m^2/g).[13] This difference may perhaps be attributed to the smaller amount of silicon in **1**. However, the surface area of uncalcined **CrOSi$_{xg}$** is higher than that of the xerogel generated via the solution thermolysis of {Me$_2$Al[μ-OSi(O^{t}Bu)$_3$]}$_2$ (210 m^2/g).[8] The surface area of **CrOSi$_{xg}$** was substantially reduced after calcination at 400 °C (to 180 m^2/g), but a slight increase in the surface area occurred with further calcination at 500 °C (205 m^2/g). This increase in surface area was coincident with both the color change from brown to green and the onset of the 6% weight loss, indicating the removal of residual organics from the surface of the material.[8] Indeed, elemental analysis revealed that the carbon contents of **CrOSi$_{xg}$** samples calcined at 200 and 500 °C were 3.85 and 0.56%, respectively. The surface area of **CrOSi$_{xg}$** continued to decrease, as expected, upon further calcination in O_2.

Interestingly, t-plot analyses suggest that the micropore contribution to the total surface area drops sharply from the uncalcined xerogel to that calcined at 400 °C, but rises again after calcination at 500 °C (Table 5). The mesopore contribution to the total surface area of **CrOSi$_{xg}$** appears to decline steadily throughout the calcination procedure, in contrast to the situation for **CrOSi$_{ss}$**, which exhibits a steady increase in the mesopore contibution to the total surface area with calcination. The total pore volume for uncalcined **CrOSi$_{xg}$** (0.31 cm^3/g) was ca. 50% higher than that observed for **CrOSi$_{ss}$**. At higher calcination temperatures, the pore volume decreased more rapidly for **CrOSi$_{xg}$**, indicating

---

[37] Weckhuysen, B. M.; Wachs, I. E. *J. Phys. Chem.* **1996**, *100*, 14437.

[38] (a) Tanev, P. T.; Pinnavaia, T. J. *Chem. Mater.* **1996**, *8*, 2068. (b) Zhang, W.; Pauly, T. R.; Pinnavaia, T. J. *Chem. Mater.* **1997**, *9*, 2491. (c) Pauly, T. J.; Liu, Y.; Pinnavaia, T. J.; Billinge, S. J. L.; Rieker, T. P. *J. Am. Chem. Soc.* **1999**, *121*, 8835.

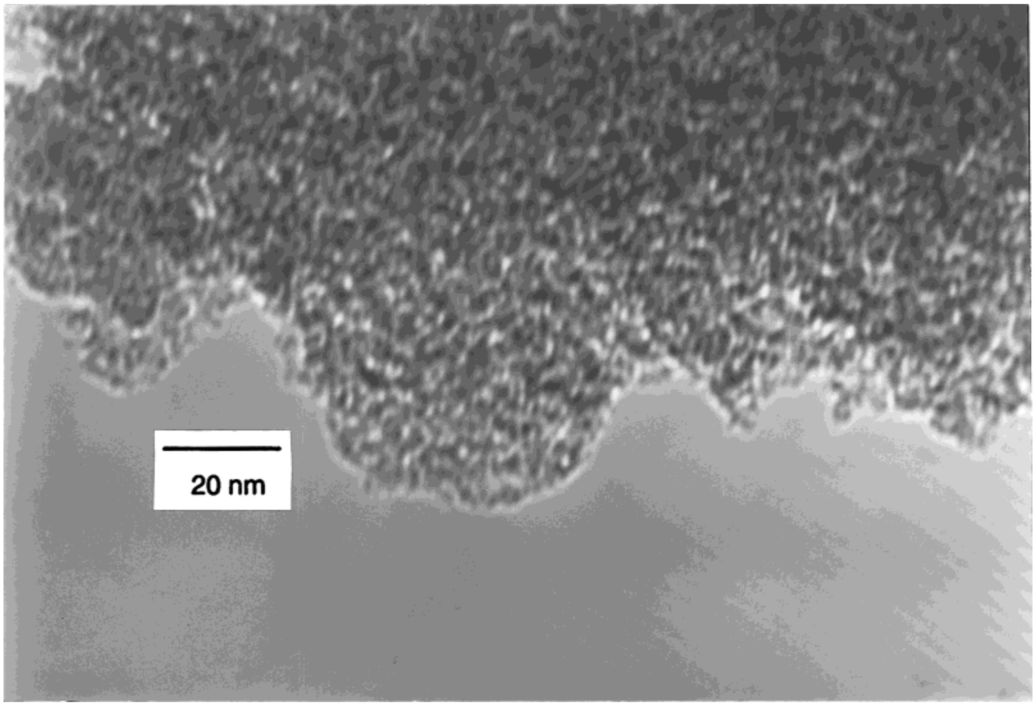

Figure 10. TEM image of **CrOSi$_{xg}$** after calcination at 200 °C under a flow of oxygen.

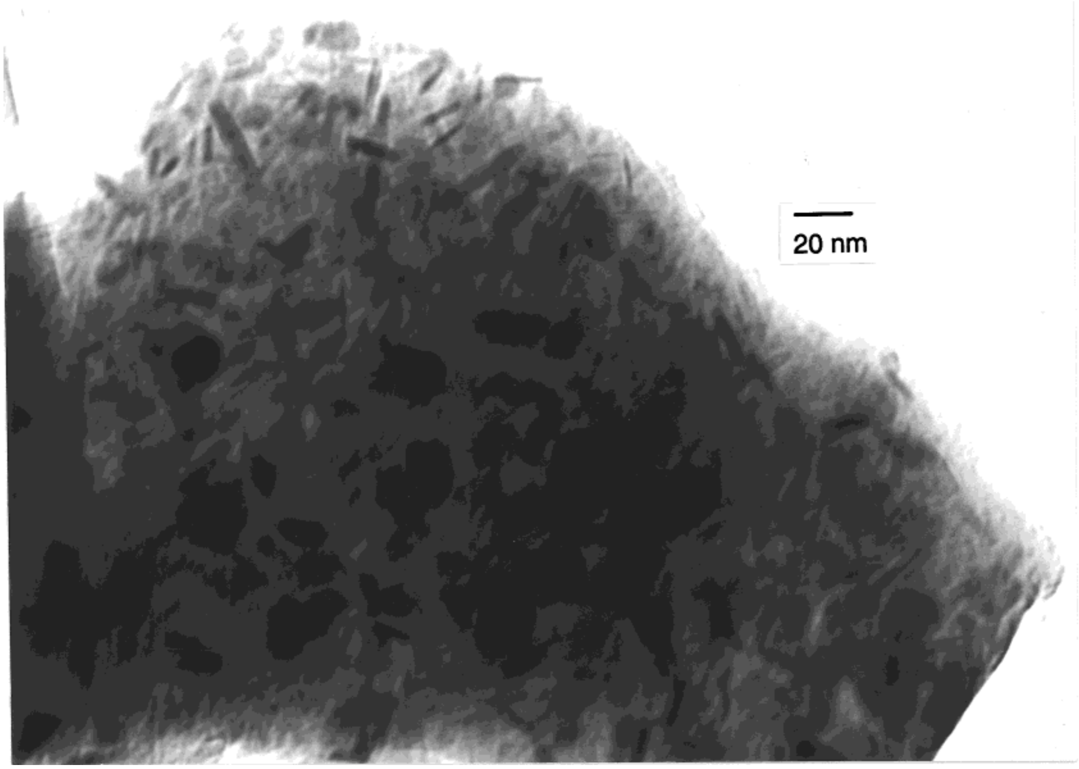

Figure 11. TEM image of **CrOSi$_{xg}$** after calcination at 1200 °C under a flow of oxygen.

greater pore collapse and thermal instability. Elemental analysis of **CrOSi$_{xg}$** after calcination at 200 °C determined that the Cr:Si ratio was nearly 1:1 (0.94:1), indicating a relatively clean conversion to a Cr/Si/O material.

Oxidative Dehydrogenation of Propane. The chromia−silica materials derived from **1** and calcined at 500 °C were examined as catalysts for the oxidative dehydrogenation (ODH) of propane to propene. Although Cr oxides are better known as dehydrogenation catalysts,[23] our recent interest in the ODH of propane[14,17,19] prompted us to examine **CrOSi$_{ss}$** and **CrOSi$_{xg}$** as ODH catalysts. The ODH reactions were run in a fixed-bed flow reactor using a propane-rich feed to ensure that propane was in large excess. Data corresponding to low propane conversions (≤10%) were collected to allow for the accurate determination of intrinsic activities and selectivities, by extrapolation to

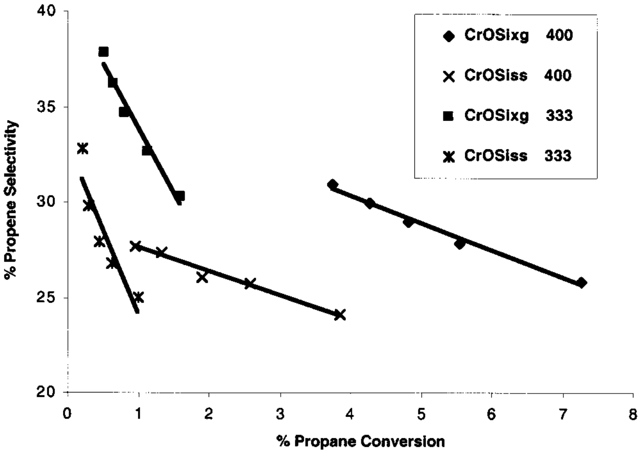

Figure 12. % Selectivity for propene versus % conversion of propane for the ODH of propane using the materials derived from **1** as catalysts. Reaction temperatures of 400 and 333 °C. Mass of catalyst used: **CrOSi$_{ss}$** = 0.010 g; **CrOSi$_{xg}$** = 0.015 g.

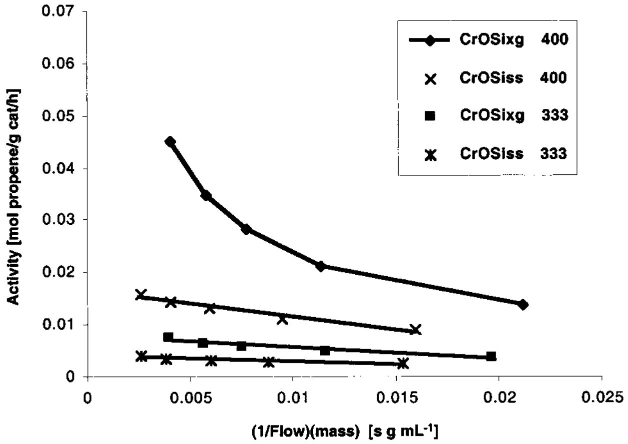

Figure 13. Activity versus the product of 1/flow and the mass of catalyst used for the ODH of propane using materials derived from **1** as catalysts. Reaction temperatures of 400 and 333 °C.

0% conversion (for selectivity) or infinite flow rate (for activity). This method of reporting activity and selectivity data has been shown by Iglesia, Bell, and co-workers to be a useful way to compare ODH catalysts.[39,40]

Figure 12 provides data on the selectivities for propene formation at reaction temperatures of 333 and 400 °C. Clearly, the selectivity for the production of propene (vs combustion of propane and propene) was highest for **CrOSi$_{xg}$**. Figure 13 presents a plot of activity (in mole of propene produced per gram of catalyst per hour of reaction time) as a function of conversion (plotted as the product of the reciprocal flow rate and the mass of catalyst used, thus normalizing for the mass of each catalyst). From these data, it is also clear that **CrOSi$_{xg}$** exhibits the higher activity as a catalyst for propane ODH. In fact, the intrinsic activity for **CrOSi$_{xg}$** at 333 °C is nearly 2 times that of **CrOSi$_{ss}$**, and at 400 °C it is nearly 3 times higher (Table 7). The data in Table 7 show that, at various measured conversions of propane, the xerogel performs even better relative to **CrOSi$_{ss}$**.

Table 7. Summary of the ODH Reactions Using the Materials Derived from 1

reaction temp (°C)	intrinsic activity[a]	intrinsic % selectivity[b]	activity at 0.5 or 4%[c]	% selectivity at 0.5 or 4%[c]	ratio of CO_2 vs CO[d]
			CrOSi$_{xg}$		
333	7.8	41	7.1	37.9	4.1:1
400	44.8[e]	36	37.8	30.3	3.5:1
			CrOSi$_{ss}$		
333	4.1	33	3.3	28.6	4.0:1
400	16.6	29	8.6	23.9	3.3:1

[a] Units: mmol of C_3H_6 produced per gram of catalyst per hour of reaction. [b] Selectivity for C_3H_6 production based on C_3H_8 converted. [c] Conversions of propane for the reactions are 0.5% at 333 °C and 4% at 400 °C. [d] Values given are for the lowest flow of reactants at the given temperature; however, the selectivities for CO_2 were the same or only slightly better at higher flow rates. [e] This value is associated with considerable error, given the curvature of the activity plot (see Figure 13) and is probably an underestimation.

Table 8. Summary of the Kinetic Data for the ODH Reactions at an Operating Temperature of 333 °C Using Catalysts Derived from 1

catalyst	k_1 (L mol^{-1} s^{-1})	k_2 (L mol^{-1} s^{-1})	k_3 (L mol^{-1} s^{-1})	k_2/k_1	k_3/k_1
CrOSi$_{xg}$	0.073	0.118	3.09	1.60	42.1
CrOSi$_{ss}$	0.037	0.076	4.66	2.06	127

Both catalysts displayed a favorable selectivity for the formation of CO_2 versus CO, indicating that the combustion processes are relatively clean (Table 7).

Further insight into the behavior of **CrOSi$_{xg}$** and **CrOSi$_{ss}$** can be gained via kinetic analyses of the catalytic reactions. It has been shown that propane reacts with oxygen in parallel and sequential steps over metal oxide catalysts (eq 3).[39−43] If the oxygen conversion is kept low, pseudo-first-order rate coefficients for the oxidative dehydrogenation step (k_1), the primary combustion of propane (k_2), and the secondary combustion of propene (k_3) can be obtained.[39] These rate constants define the key parameters that allow comparisons of catalyst performance.

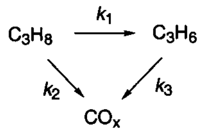

(3)

The results of these kinetic analyses (Table 8) show that the rate of propane ODH (k_1) at 333 °C is higher for **CrOSi$_{xg}$** by a factor of ca. 2. A comparison of the k_2/k_1 ratios, a measure of the relative activity for the combustion of propane versus the ODH of propane, indicates that **CrOSi$_{xg}$** exhibits a lower relative activity for propane combustion. However, the actual rate of propane combustion (k_2) for **CrOSi$_{xg}$** is higher than that for **CrOSi$_{ss}$**. Signficantly, the data of Table 8 (in particular, the k_3/k_1 ratios) indicate that the superior performance of **CrOSi$_{xg}$** is largely due to its lower activity for propene combustion.

---

(39) Khodakov, A.; Yang, J.; Su, S.; Iglesia, E.; Bell, A. T. *J. Catal.* **1998**, *177*, 343.

(40) Khodakov, A.; Olthof, B.; Bell, A. T.; Iglesia, E. *J. Catal.* **1999**, *181*, 205.

(41) Albonetti, S.; Cavani, F.; Trifiro, F. *Catal. Rev.-Sci. Eng.* **1996**, *38*, 413.

(42) Blasco, T.; Lopez Nieto, J. M. *Appl. Catal. A* **1997**, *157*, 117.

(43) Chen, K.; Bell, A. T.; Iglesia, E. *J. Phys. Chem. B* **2000**, *104*, 1292.

It is interesting that different catalytic properties (for **CrOSi$_{xg}$** and **CrOSi$_{ss}$**) arise simply from the different manner in which the molecular single-source precursor is thermolytically converted to the material. The inherent selectivities for the catalysts suggest that the two preparative methods result in different active sites or differences in the distributions of various sites. The present results do not allow us to interpret these differences in terms of active site structures. However, several research groups have proposed that the active sites in oxide-supported chromium dehydrogenation and oxidative dehydrogenation catalysts are coordinatively unsaturated Cr(III) centers.[23] Jiménez-López et al. have shown that bulk Cr_2O_3 has only moderate activity for the ODH of propane due to the lack of accessible active Cr centers, presumably due to a low surface area.[23f,g] The main difference between the catalysts derived from **1** is that **CrOSi$_{ss}$** is more homogeneous (by PXRD analysis and IR spectroscopy) and has a higher thermal stability (by BET analysis), while **CrOSi$_{xg}$** has more nanocrystalline Cr_2O_3 domains corresponding to a lower thermal stability for highly dispersed, homogeneous structures. This suggests that the more active and selective ODH sites of **CrOSi$_{xg}$** are derived from nanocrystalline chromia domains, rather than from Cr−O−Si species, which are expected to be more abundant in **CrOSi$_{ss}$**. Both of the catalysts derived from **1** have relatively high surface areas, resulting in accessible catalytic Cr sites and hence high activity for the ODH reaction.

Conclusions

Synthetic routes to the first chromium(IV) alkoxysiloxy complexes (**1** and **2**) have presented the opportunity to examine thermolytic molecular precursor routes to relatively carbon-free chromia−silica materials. The materials obtained from solid-state thermolyses of complex **1** (**CrOSi$_{ss}$**) exhibit high surface areas and high thermal stabilities, as demonstrated by little reduction in surface area and pore volume even after calcination at 500 °C. Low-temperature solution thermolyses of **1** result in high surface area Cr/Si/O xerogels (**CrOSi$_{xg}$**) that display a loss of ca. 30% in area and pore volume after calcination at 500 °C. By TEM and PXRD analyses and IR spectroscopy, **CrOSi$_{ss}$** appears to be rather homogeneous, in that crystalline Cr_2O_3 is not observed until heating to >600 °C.[13] By this criterion, **CrOSi$_{xg}$** is somewhat less homogeneous because it exhibits an earlier phase separation and crystallization of Cr_2O_3, possibly as a consequence of the formation of more Cr−O−Cr linkages during the solution thermolysis.

Although they are not exceptional propane ODH catalysts, the materials generated from **1** exhibit interesting differences in activity and selectivity for the ODH of propane, with **CrOSi$_{xg}$** performing better in both respects. Kinetic analyses suggest that these catalysts are characterized by fundamental differences in the nature of the catalytic centers, despite the fact that they are generated by thermolysis of the same single-source molecular precursor (**1**). Future reports will describe molecular precursor routes to supported Cr−O−Si catalysts for the conversion of propane to propene.

Experimental Section

General. All synthetic manipulations were performed under an atmosphere of nitrogen using standard Schlenk techniques and/or a Vacuum Atmospheres drybox, unless noted otherwise. All solvents used were distilled from sodium/benzophenone, potassium/benzophenone, sodium, or calcium hydride as appropriate. The ^1H NMR spectra were recorded using Bruker AMX300 (at 300 MHz) or Bruker DRX500 (at 500 MHz) spectrometers. Benzene-d_6, vacuum transferred from a Na/K alloy, was used as the solvent for all NMR studies. Infrared spectra were recorded using a Mattson Infinity Series FTIR spectrometer with all samples being pressed into KBr disks. Thermal analyses were performed using a TA Instruments SDT 2960 integrated thermogravimetric/differential thermal analyzer (TGA/DTA). Surface area and pore volume analyses were performed using a Quantachrome Autosorb 6 surface area analyzer with all samples heated at 120 °C, under vacuum, for a minimum of 4 h immediately prior to data collection. X-ray powder diffraction data were obtained using a Siemens D5000 diffractometer operating with $\theta - 2\theta$ geometry at room temperature. The PXRD data were collected using Cu Kα radiation ($\lambda = 1.5406$ Å), a collection time of 1.5 s, and a step size of 0.02°. Magnetic susceptibility measurements from 5 to 200 K were performed using a Quantum Design Magnetic Property Measurement System (MPMS) equipped with a SQUID detection system. Transmission electron microscopic images were obtained using a JEOL 200cx transmission electron microscope at an operating accelerating voltage of 200 kV. Samples for TEM analyses were prepared via deposition using a pentane suspension of finely ground material on a "Type A" carbon-coated copper grid obtained from Ted Pella Inc. Elemental analyses on **1** and **2** were performed by the College of Chemistry Micro-Mass Facility at the University of California, Berkeley. Elemental analyses of **CrOSi$_{ss}$** and **CrOSi$_{xg}$** were performed by Mikroanalytisches Labor Pascher, Germany (Cr and Si) and by the College of Chemistry Micro-Mass Facility (C and H). Fast atom bombardment mass spectrometric analyses, in the presence of a matrix (NBA), were recorded by the College of Chemistry Micro-Mass Facility. Single-crystal X-ray structure determinations were performed by the UCB College of Chemistry X-ray facility (CHEXRAY). Chromium tetrakis(*tert*-butoxide),[30] $CrCl_3(THF)_3$,[44] and $HOSi(O^tBu)_3$[45] were prepared by literature procedures.

$(^tBuO)_3CrOSi(O^tBu)_3$ (1). (a) A toluene solution (10 mL) of $HOSi(O^tBu)_3$ (0.221 g, 0.836 mmol) was added to a toluene solution (10 mL) of $Cr(O^tBu)_4$ (0.288 g, 0.836 mmol) at room temperature in a Schlenk tube. The resulting mixture was heated to 80 °C and stirred for 12 h under a flow of N_2. The solvent and volatile impurities were removed under reduced pressure in two stages: at room temperature and then subsequently at 50 °C. Sublimation of the remaining dark blue solid residue at 80 °C yielded 0.266 g (0.497 mmol, 59%) of **1**. A portion of the sublimed product was recrystallized from a 1:1 mixture of toluene and acetonitrile for subsequent analyses.

(b) A more convenient and higher yielding preparation for **1** involved heating a solid mixture of $Cr(O^tBu)_4$ (0.887 g, 2.58 mmol) and $HOSi(O^tBu)_3$ (0.681 g, 2.58 mmol) to 80 °C (above the melting point of both compounds) for 30 min under a nitrogen flow in a Schlenk tube. The Schlenk tube containing the reaction mixture was cooled to 50 °C and the volatile components were then removed under reduced pressure. The residual dark blue solid was recrystallized from a 1:1 mixture of toluene and acetonitrile at −30 °C and subsequently washed with cold acetonitrile to afford 1.115 g (2.09 mmol, 81%) of analytically pure blue platelike crystals of **1**.

Anal. Calcd for $C_{24}H_{54}CrO_7Si$: C, 53.90; H, 10.18. Found: C, 53.89; H, 10.44. IR (cm^{-1}): 2975 vs, 2929 m, 2903 w, 2872 w, 1473 w, 1457 w, 1387 w, 1363 s, 1241 m, 1193 s, 1163 s, 1059 vs, 1028 m, 990 m, 925 vs, 907 s, 830 w, 787 m, 701 w, 670 vw, 626 w, 475 w. ^1H NMR (benzene-d_6, 500 MHz) δ 1.68

---

(44) Herwig, W.; Zeiss, H. H. *J. Org. Chem.* **1958**, *23*, 1404.

(45) Abe, Y.; Kijima, I. *Bull. Chem. Soc. Jpn.* **1969**, *42*, 1118.

(s br, 27 H, $OSi(O^tBu)_3$), 3.41 (s vbr, 27 H, $Cr(O^tBu)_3$). FAB-MS: *m/z* 534 (M^+). mp 108−110 °C dec $\mu_{eff} = 2.80\ \mu_B$.

$CrOSi_{ss}$. In a representative solid-state thermolysis, a Schlenk tube charged with **1** (0.137 g, 0.256 mmol) was heated to 180 °C under an atmosphere of N_2. The evolution of a gas was observed with a corresponding change in color of the solid from blue to brown. The solid was then heated for an additional 30 min to ensure complete conversion of **1**. The Schlenk tube containing the brown solid was cooled to room temperature, and solid **$CrOSi_{ss}$** was collected in the air (0.033 g, 24.1%). Calcinations for PXRD analyses were conducted by heating samples at 10 °C/min under flowing O_2 (100 cm^3/min) to the desired temperature, which was maintained for 30 min using either an SDT 2960 thermal analyzer or a Lindberg 1200 °C three-zone tube furnace. Surface area measurements were performed on samples calcined at 10 °C/min under flowing O_2 (100 cm^3/min) to a given temperature, which was maintained for 1 h in a Lindberg 1200 °C three-zone tube furnace. Small-scale solid-state thermolyses were conducted in the furnace of an SDT 2960 thermal analyzer under Ar with a flow rate of 100 cm^3/min. The ceramic yield when heated under an argon atmosphere was 24.4%.

$CrOSi_{xg}$. A representative experiment consisted of a solution of **1** (0.400 g, 0.748 mmol) in *n*-octane (8.0 mL) that was sealed in a 100-mL thick-walled Pyrex pyrolysis tube after three freeze−pump−thaw cycles. The tube was then placed in a preheated oven at 180 °C for 24 h, until gel formation was observed. The light green gelatinous precipitate that formed was air-dried for 3 days, yielding **$CrOSi_{xg}$** (0.123 g, 31% ceramic yield). Calcination of the xerogel was performed in the furnace of an SDT 2960 thermal analyzer (small scale) or in a Lindberg 1200 °C three-zone tube furnace under flowing oxygen at 100 cm^3/min. The temperature was ramped at 10 °C/min to the desired value, which was maintained for 30 min for PXRD studies and 1 h for BET measurements.

$(^tBuO)_2Cr[OSi(O^tBu)_3]_2$ (2). A solid mixture of $Cr(O^tBu)_4$ (0.252 g, 0.732 mmol) and $HOSi(O^tBu)_3$ (0.387 g, 1.46 mmol) was heated to 80 °C for 1 h under a flow of nitrogen in a Schlenk tube. The resulting mixture was cooled to 50 °C and the volatile impurities were removed under reduced pressure. The remaining blue solid/oil was dissolved in a 1:1 mixture of toluene and acetonitrile and cooled to −30 °C. Thin blue/green analytically pure crystals of **2** (0.359 g, 68%) were obtained after washing with cold acetonitrile. Anal. Calcd for $C_{32}H_{72}CrO_{10}Si_2$: C, 53.00; H, 10.01. Found: C, 53.30; H, 10.39. IR (cm^{-1}): 2975 vs, 2931 m, 2903 w, 2874 w, 1473 w, 1389 m, 1365 s, 1242 m, 1193 s, 1062 vs, 1028 m, 926 s, 907 s, 830 m, 788 m, 701 m, 670 vw, 626 w, 511 w, 477 w. ^1H NMR (benzene-d_6, 300 MHz) δ 1.70 (s br, 54 H, $[OSi(O^tBu)_3]_2$), 3.43 (s br, 18 H, $Cr(O^tBu)_2$). FAB-MS: *m/z* 724 (M^+). $\mu_{eff} = 2.71\ \mu_B$.

Solid-State Thermolyses of 2. Solid-state thermolyses were conducted by heating samples at 10 °C/min, under a flow of Ar at 100 cm^3/min, to the desired temperature in the furnace of an SDT 2960 thermal analyzer. The ceramic yield was 26.6%.

NMR Study of the Solution Thermolyses of 1 and 2. Compound **1** (11.5 mg, 0.021 mmol) and ferrocene (12.1 mg, 0.065 mmol) were dissolved in benzene-d_6 and sealed in an NMR tube after three freeze−pump−thaw cycles. The tube was heated to 180 °C for 1 h, until thermolysis was evident. The soluble decomposition products were quantified by integration against the ferrocene standard: $CH_2{=}CMe_2$ (0.098 mmol); ^tBuOH (0.002 mmol); H_2O (0.01 mmol). Compound **2** (5.8 mg, 0.008 mmol) and ferrocene (4.0 mg, 0.022 mmol) were treated similarly to give the following soluble products: $CH_2{=}CMe_2$, 3.7 mg (0.061 mmol); ^tBuOH, 0.4 mg (0.006 mmol); H_2O, 0.1 mg (0.006 mmol).

Oxidative Dehydrogenation of Propane. Selectivites and conversions for the oxidative dehydrogenation of propane were measured using a fixed-bed flow reactor (quartz) fitted with a medium frit. The mass of catalyst used was 0.010 g for **$CrOSi_{ss}$** and 0.015 g for **$CrOSi_{xg}$**. Quartz powder (0.500 g, 0.246−0.494 mm) was used to disperse each catalyst within the reactor. The gas stream consisted of helium (200 cm^3/min), propane (25 cm^3/min), nitrogen (2 cm^3/min), and oxygen (9 cm^3/min). The gaseous reactants and products were analyzed online using a Hewlett-Packard 6890 gas chromatograph equipped with both a capillary column (HP-1) and a packed column (HAYESEP-Q). Only C_3H_6, CO, CO_2, and H_2O were detected as reaction products. Propane and oxygen conversions were varied by changing the total flow rate (between 50 and 236 cm^3/min). The reaction was run at temperatures of 333 and 400 °C for each catalyst. Typical propane conversions ranged from 0.2 to 7.5% with oxygen conversions of 2% for the least active conditions (333 °C at high flow rates) and 72% for the most active conditions (400 °C at low flow rates).

Structure Determinations for 1 and 2. X-ray quality crystals of **1** or **2** were grown from a mixture of toluene and acetonitrile (1:1) that was cooled to −30 °C. A thin fragment of a blue platelike crystal of **1** having approximate dimensions of 0.50 × 0.30 × 0.01 mm or a thin fragment of a bluish/green platelike crystal of **2** having approximate dimensions of 0.40 × 0.30 × 0.02 mm was selected for analysis. Each crystal was mounted on a quartz fiber using Paratone N hydrocarbon oil. All measurements were made on a SMART CCD area detector with graphite monochromated Mo Kα radiation. Cell constants and an orientation matrix were obtained from a least-squares refinement using the measured positions of 2299 reflections in the range $3.00 < 2\theta < 46.00°$ for **1** and 3919 reflections in the range $3.00 < 2\theta < 46.00°$ for **2**. The data were collected at a temperature of -95 ± 1 °C for **1** and -120 ± 1 °C for **2**. Frames corresponding to an arbitrary hemisphere of data were collected using ω scans of 0.3° counted for a total of 10.0 s per frame. Data were integrated using the program SAINT to a maximum 2θ value of 41.6° for **1** and 49.4° for **2**. The data were corrected for Lorentz and polarization effects. Data were analyzed for agreement and possible absorption using XPREP. An empirical absorption correction based on comparison of redundant and equivalent reflections was applied using SADABS ($T_{max} = 0.98$, $T_{min} = 0.66$ for **1** and $T_{max} = 0.96$, $T_{min} = 0.65$ for **2**). The structures were solved by direct methods and expanded using Fourier techniques. All calculations were performed using the Teχsan crystallographic software package. The disorder in the Cr and Si positions for **1** was modeled such that the occupancy of Cr1 was refined (0.500(5)) and the occupancies of Cr2, Si1, and Si2 were constrained so that the sum of the Cr occupancies, the sum of the Si occupancies, and the sum of the Cr and Si atoms occupying the same site were all equal to 1. The non-hydrogen atoms of **1** and **2** were refined anisotropically. Hydrogen atoms were included in calculated idealized positions but not refined. The final cycle of full-matrix least-squares refinement for **1** was based on 1740 observed reflections ($I > 3.00\sigma(I)$) and 299 variable parameters and converged with unweighted and weighted agreement factors of $R(F) = 0.054$, $R_w(F) = 0.056$, and GOF = 1.94. The final cycle of full-matrix least-squares refinement for **2** was based on 3162 observed reflections ($I > 3.00\sigma(I)$) and 406 variable parameters and converged with unweighted and weighted agreement factors of $R(F) = 0.046$, $R_w(F) = 0.045$, and GOF = 1.48.

Acknowledgment. This work was supported by the Director, Office of Energy Research, Office of Basic Energy Sciences, Chemical Sciences Division, of the U.S. Department of Energy under Contract DE-AC03-76SF00098. We also thank Professors E. Iglesia (BET), A. Stacy (PXRD and MPMS), and A. Bell (Raman) for the use of instrumentation.

Supporting Information Available: Tables of crystal, data collection, refinement parameters, bond distances and angles, and anisotropic displacement parameters for **1** and **2** (PDF). This material is available free of charge via the Internet at http://pubs.acs.org.

CM010027X